J Supercond Nov Magn (2012) 25:2297–2307
DOI 10.1007/s10948-012-1629-7

ORIGINAL PAPER

The Effect of PbSe Addition on the Mechanical Properties of Bi-2212 Superconductors

S. Cavdar · E. Deniz · H. Koralay · O. Ozturk · M. Erdem · A. Gunen

Received: 20 April 2012 / Accepted: 8 May 2012 / Published online: 31 May 2012

Abstract The effects of PbSe addition and heat treatment on the structure and mechanical properties of Bi-2212 superconductors are analyzed. Glass ceramic method is used to produce PbSe added samples. The mechanical properties are derived using Vickers microhardness measurement results. Well known analysis methods like Meyer's law, *PSR* (Proportional Sample Resistance) Model, *EDP* (Elastic/Plastic Deformation Model), Hays-Kendall approach and *IIC* (Indentation-Induced Cracking Model) are used to calculate load independent microhardness values of the samples. HK approach produces successful results for the samples A, E, F, G and H indicating *ISE* (Indentation Size Effect) behavior. The *IIC* model successfully explains *RISE* (Reverse Indentation Size Effect) behavior for the samples B, C and D. *RISE* behavior is observed only for the samples where the plastic deformation is dominant. *ISE* behavior is observed for the samples where both elastic and plastic deformation are produced. The results of XRD and SEM analysis show improvement with PbSe addition in the crystal structures and surface morphologies of superconducting samples.

S. Cavdar (✉) · E. Deniz · H. Koralay · A. Gunen
Superconductivity and Thermal Analysis Laboratory,
Department of Physics, Faculty of Science, Gazi University,
06500 Ankara, Turkey
e-mail: cavdar@gazi.edu.tr

O. Ozturk
Department of Physics, Faculty of Arts and Sciences,
Kastamonu University, 37100 Kastamonu, Turkey

M. Erdem
Department of Physics, Faculty of Arts and Sciences, Abant Izzet
Baysal University, 14280, Bolu, Turkey

Keywords XRD · SEM · Bi-2212 · Vickers microhardness · ISE · RISE

1 Introduction

The mechanical properties like hardness, elasticity, ductility and toughness of materials are as vital as the superconducting properties like critical temperature, critical current density and critical magnetic field for industrial applications in the form of wires and tapes. Engineering applications of high temperature superconducting ceramics are generally restricted because of their brittleness nature; therefore improvement of the mechanical properties of *BSCCO* is a major research objective and very important for their practical applications. Hardness is the measure of the resistance of a material against a load applied to its surface. Hardness measurements are nondestructive and easy to perform and are commonly used to evaluate the quality of produced materials in industry. Hardness is a mechanical property and it is strongly related to the composition and structure of solids. Therefore, the hardness tests are popular to characterize materials [1–4]. Vickers hardness testing is commonly used to analyze the hardness of most materials and produce convenient results. If the deformation is due to very small applied loads, elastic deformation is observed. Forces above some critical value produce plastic (irreversible) deformation.

It is well known that the microhardness of solids depends on the applied load. Generally, the microhardness value decrease with increase in the applied load, which is known as *ISE* (Indentation Size Effect). Another case is *RISE* (Reverse Indentation Size Effect), where the microhardness increases with applied load. In this study, we analyzed the effect of PbSe addition and heat treatment on the mechanical properties of Bi-2212 samples, and we employed various models to

extract load independent microhardness values of the samples.

2 Experimental Procedure

PbSe added $Bi_2Sr_2CaCu_2(PbSe)_xO_y$ samples with $x = 0, 0.1, 0.3$ and 0.5 were prepared by glass ceramic method using high purity Bi_2O_3, $SrCO_3$, $CaCO_3$, CuO and PbSe chemicals. The powders are mixed for 1 hour in agate mortar and then melted for 3 hours at 1150 °C. The molten phase is quenched between pre-cooled copper plates to produce 0.5–0.8 mm thick glasses. The glass products are sintered at 845 °C for 120 hours to obtain the superconducting crystal structure. For simplicity, the glass products PbSe0, PbSe01, PbSe03, PbSe05 will be called A, B, C and D and the superconducting samples FPbSe0, FPbSe01, FPbSe03, FPbSe05 will be called E, F, G and H, respectively.

The phase compositions are characterized by *XRD* investigation by Bruker D8 Advance *XRD* with CuK_α radiation ($\lambda = 1.5418$ Å) in the range $2\theta = 4$–$70°$ at a scan speed of 3 °/min and a step increment of 0.02° at room temperature. Phase ratio and lattice parameters a and c of the samples are determined from the high-angle (00l) peaks of the XRD patterns. The relative volume fractions of the *Bi-2212* and *Bi-2201* phases were determined from the peak intensities of the same particular reflections. Additionally, the average particle sizes of the samples produced are computed with the aid of the Scherrer–Warren approach. The surface morphologies of the sample are studied by using a TESCAN scanning electron microscope (SEM) to determine the grain sizes and possible precipitation at the grain boundaries.

The Vickers microhardness measurements are taken at room temperature with Shimadzu HVM-2 model digital microhardness tester. The applied load (F) varied in the range 0.245–2.940 N and applied for 10 seconds. The indenter was pressed on the polished different surfaces of the samples making sure that the indentations do not overlap. Vickers microhardness results and the previously mentioned microhardness models are used to determine the load independent microhardness values of the samples.

3 Result and Discussion

3.1 XRD Analysis

XRD peaks of the samples are shown in Fig. 1. Sample H has the highest intensity peaks among PbSe added superconducting samples. The increase in the peak intensity can be associated with the increase in grain sizes. The fraction of Bi-2212 phase in sample H is higher than that of sample E (Table 1). There is a small amount of Bi-2201 phase but the dominant phase is Bi-2212 phase. From Table 1 we can conclude that addition of PbSe enhances the formation of Bi-2212 phase. The lattice parameters a and c are calculated using least squares method for orthorhombic structure and the results are tabulated in Table 1. The lattice parameter a decreases monotonically, while the lattice parameter c increases with addition. The results show that the structural properties of superconducting samples improve with addition.

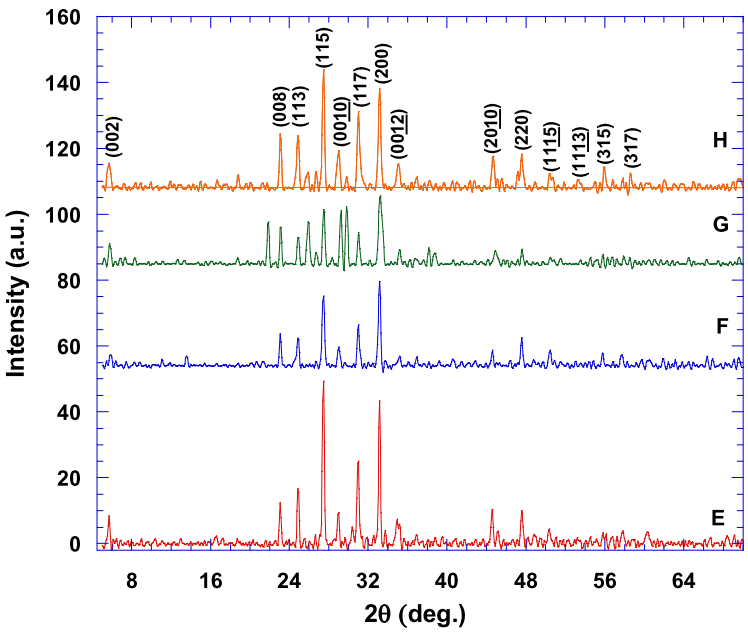

Fig. 1 XRD patterns of the E, F, G and H samples

Table 1 Lattice parameter a and c, volume fraction and grain size of the all samples

Samples	a (Å)	c (Å)	Volume fraction (%)		Grain size (nm)
			2212	2201	
E	5.40	30.61	91	9	47.25
F	5.38	30.66	94	6	49.70
G	5.37	30.69	95	5	57.46
H	5.35	30.71	98	2	71.13

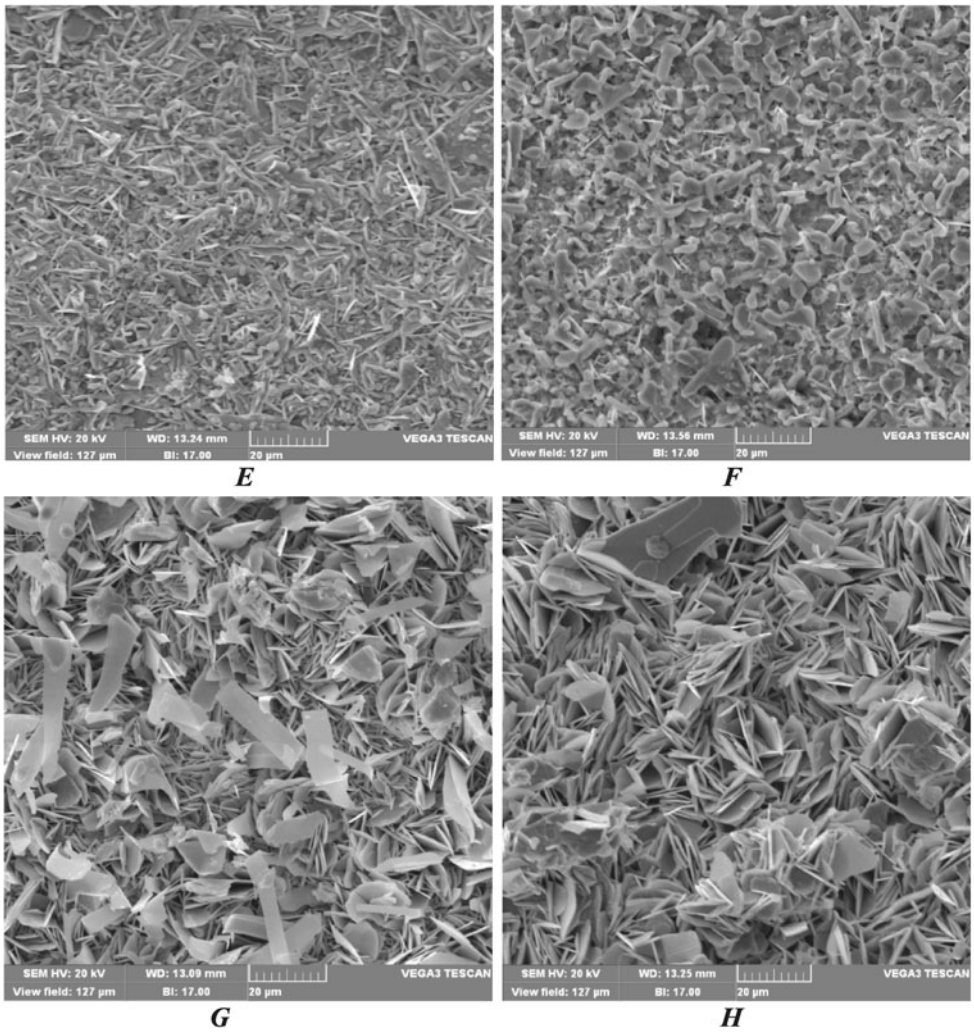

Fig. 2 SEM micrographs of all samples

3.2 Grain Size Calculation

The average grain sizes of the samples are calculated from the XRD patterns and using Scherrer–Warren equation.

$$D = 0.941\lambda/\beta\cos\theta_\beta \tag{1}$$

where D is the grain size, λ is the wavelength of X ray, β is the FWHM (full width at half maximum) of the highest intensity peak, and θ is the corresponding angle of the peak. The results of the calculations are tabulated in Table 1. As seen from the table, the average grain sizes of the superconducting samples increase with addition. This result is consistent with the *SEM* images of the samples.

3.3 SEM Analysis

So as to determine the grain sizes and possible precipitation at the grain boundaries, the structure of surface morphology of the samples are studied by SEM. Figure 2 shows the SEM images of the samples E, F, G and H. From the images it is seen that with increase in addition, the grain size increase and porosities between grains decrease. The sample H is denser and has less porosity. Since porosity decreases with

addition, the grains approach one another and so the grain connectivity enhances. The increase in grain sizes is also confirmed by the grain size calculations using XRD peaks.

3.4 Vickers Microhardness Measurements

The indentation sizes are measured and load dependent microhardness, elastic modulus, yield strength and fracture toughness values are calculated using (2)–(5).

$$H_v = 1854.4\left(\frac{F}{d^2}\right)\ (\text{GPa}) \tag{2}$$

$$E = 81.9635 H_v \tag{3}$$

$$Y \approx \frac{H_v}{3} \tag{4}$$

$$K_{\text{IC}} = \sqrt{2E\alpha} \quad (\alpha, \text{surface energy}) \tag{5}$$

The results are tabulated in Table 2. From the table it is clear that for all samples the microhardness values depend on the applied load. For samples A, E, F, G and H the microhardness value decreases with increasing applied load. This kind of nonlinear microhardness—load behavior is called indentation size effect (*ISE*) in the literature [5, 6].

- Smaller values of loads exhibit higher values of hardness.
- Higher values of applied loads exhibit smaller values of hardness. This observation is associated with the weak grain boundaries of the ceramic materials.

For samples B, C and D the microhardness values increase with increasing applied load which is known as reverse indentation size effect (*RISE*) [7, 8]. The possible cause of *RISE* behavior may be the specimen cracking [9]. Excessive cracking in the sample decreases the elasticity and thus the microhardness of the material. For these kinds of material there is no elastic recovery, but only plastic deformation is observed.

The dependence of Vickers microhardness of the samples on the applied load are displayed in Fig. 3. For all samples exhibiting either *ISE* or *RISE* behavior, for higher applied loads the load dependence of microhardness values decreases and the microhardness values converge to a plateau of rather constant microhardness value. The microhardness values at the plateau region are considered to be the load independent (real) hardness values [10]. The microhardness values reaches to that of the plateau region at about 1 N for F, G and H samples and about 2 N for the other samples.

For glass samples (A, B, C and D) the microhardness increases with increasing addition, but for superconducting samples (E, F, G and H) the microhardness decreases monotonically with addition. For pure samples, the transition from glass phase to superconducting phase after heat treatment causes an increase in microhardness. For the doped samples, the glass—superconductor transition leads to a significant decrease of microhardness values and behavioral transition from *RISE* to *ISE*. The decrease in microhardness due to addition may be related to the impurity phases and disorder. These lead to weakening of the bonds among grains and thus the decrease of the microhardness.

The elastic modulus (E) and yield strength (Y) values increases with PbSe addition for glass samples (A, B, C, D) but it decreases significantly for crystalline Bi2212 samples (E, F, G, H). Fracture toughness (K_{IC}) values are negative for PbSe added glass samples, but they are positive for Bi-2212 crystalline samples and decrease with addition.

Since the microhardness depends on the applied load, one may be interested in calculating the load independent (real) microhardness values. In the literature various models are proposed to calculate the real microhardness values and to investigate *ISE* and *RISE* behaviors. The results of these proposed models are then compared to the microhardness values of the plateau region. In this part of the study, Meyer's law, Proportional Sample Resistance (*PSR*) Model, Elastic/Plastic Deformation (*EPD*) Model, Hays-Kendall (*HK*) approach and Indentation-Induced cracking (*IIC*) Model will be used to calculate the load independent microhardness values of our samples.

3.4.1 Analysis According to Meyer's Law

It is a simple relation between the applied load and the indentation size:

$$F = ad^n \tag{6}$$

where n_K is Meyer number which is calculated by fitting the curves of experimental data. Meyer number n_K is a measure of *ISE* behavior. For values of n_K greater than 2, *RISE* behavior is observed; for values less than 2, *ISE* behavior is observed and for $n_K = 2$ microhardness becomes load independent which is Kick's law [2, 10–12].

In Fig. 4, $\ln F$–$\ln d$ curves of the samples are shown. The values of n_K calculated from the slope of the curves are less than 2 for samples A, E, F, G and H; but for samples B, C and D the values of n_K are greater than 2. The value of Meyer number being less than 2 for samples A, E, F, G and H confirms that their load dependent microhardness has *ISE* behavior. For samples B, C and D the value of Meyer number is greater than 2, indicating that their microhardness has *RISE* behavior. These data are summarized in Table 3.

3.4.2 Analysis According to Proportional Sample Resistance Model

Proportional Sample Resistance (*PSR*) model which is developed by Li and Bradt is successfully used for the analysis of microhardness of materials showing *ISE* behavior [13]. This model is given in (7).

Table 2 The calculated load dependent H_v, E, Y, and K_{IC} for the samples

Samples	Load (N)	H_v (GPa)	E (GPa)	Y (GPa)	K_{IC} (Pa/m$^{1/2}$)
A	0.245	4.621	378.75	1.540	3813.7
	0.490	4.245	347.94	1.415	3655.3
	0.980	2.130	174.58	0.710	2589.2
	1.960	2.068	169.50	0.689	2551.2
	2.940	1.997	163.68	0.665	2507.1
B	0.245	3.809	312.20	1.269	–1836.2
	0.490	4.233	346.95	1.411	–1935.7
	0.980	4.253	348.59	1.417	–1940.3
	1.960	4.345	356.13	1.448	–1961.2
	2.940	4.549	372.85	1.516	–2006.7
C	0.245	4.358	357.20	1.452	–2345.4
	0.490	4.689	384.33	1.563	–2432.8
	0.980	5.102	418.18	1.700	–2537.7
	1.960	5.242	429.65	1.747	–2572.3
	2.940	5.322	436.21	1.774	–2591.8
D	0.245	4.730	387.69	1.576	–964.60
	0.490	4.848	397.36	1.616	–976.56
	0.980	5.163	423.18	1.721	–1007.8
	1.960	5.383	441.21	1.794	–1029.0
	2.940	5.405	443.01	1.801	–1031.1
E	0.245	5.023	411.70	1.674	3796.0
	0.490	4.165	341.38	1.388	3456.6
	0.980	3.287	269.41	1.095	3070.7
	1.960	2.608	213.76	0.869	2735.3
	2.940	2.566	210.32	0.855	2713.2
F	0.245	1.891	154.99	0.630	897.75
	0.490	1.538	126.06	0.512	809.64
	0.980	1.537	125.98	0.512	809.38
	1.960	1.536	125.90	0.512	809.12
	2.940	1.516	124.26	0.505	803.84
G	0.245	0.821	67.292	0.273	803.74
	0.490	0.670	54.916	0.223	726.08
	0.980	0.500	40.982	0.166	627.24
	1.960	0.491	40.244	0.163	621.56
	2.940	0.453	37.129	0.151	597.02
H	0.245	0.592	48.522	0.197	599.22
	0.490	0.456	37.375	0.152	525.90
	0.980	0.459	37.621	0.153	527.63
	1.960	0.407	33.359	0.135	496.85
	2.940	0.375	30.736	0.125	476.91

$$F = \alpha d + \beta d^2 \tag{7}$$

$$\frac{F}{d} = \alpha + \beta d \tag{8}$$

where α and β values are calculated from $(F/d) - d$ graph (Fig. 5). α is the surface energy, and the change in α value is associated with the energy dispersion of the surface cracks [14]. β is a parameter used to calculate the real microhardness value. In PSR model the load independent microhardness value is calculated as

$$H_{PSR} + 1854.4\beta \tag{9}$$

The calculated values of α, β and load independent microhardness values are tabulated in Table 4. The value of α is positive for samples A, E, F, G and H which show *ISE* be-

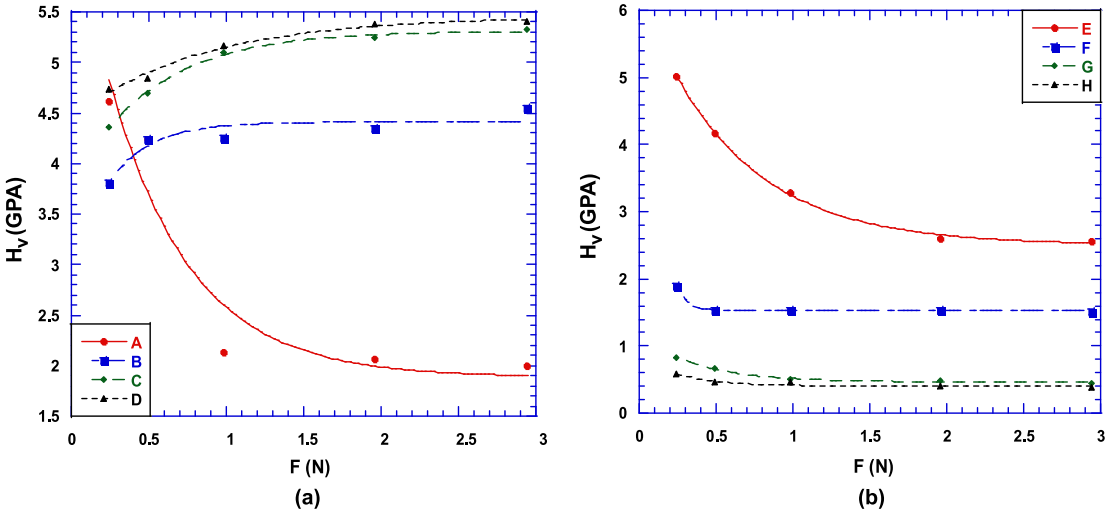

Fig. 3 The variations of microhardness with load for the samples

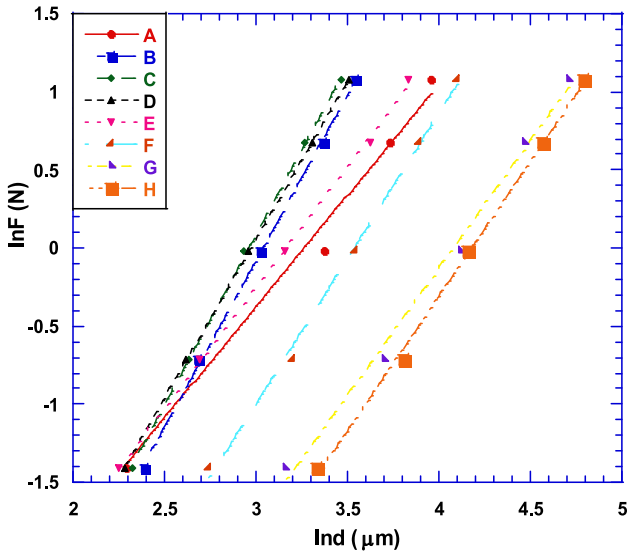

Fig. 4 Variation of applied load $\ln F$ with diagonal $\ln d$ for the samples

havior while it is negative for samples B, C and D obeying *RISE* behavior. This verifies that there is no elastic deformation for samples obeying *RISE* behavior. The microhardness values of the samples calculated using *PSR* model are far from the values of the plateau region [10, 15, 16]. Therefore, *PSR* model is invalid in computing the load independent microhardness values of our samples.

The values of load independent elastic modulus (E), yield strength (Y) and fracture toughness (K_{IC}) are calculated using load independent H_{PSR} values and are also tabulated in Table 5. When compared to the load dependent values, load independent E_0, Y_0 and K_{IC} values decrease for samples A, E, F, G and H which obey *ISE* behavior, but they increase for samples B, C and D obeying *RISE* behavior. The increase in K_{IC} value is associated with the increase in the value of surface energy α. Fracture toughness (K_{IC}),

Table 3 Best-fit results of experimental data according to Meyer's law

Samples	n_K	$\ln A_{1K}$ (GPa)	H_V (GPa)
A	1.42	–4.64	1.997–2.068
B	2.12	–6.46	4.345–4.549
C	2.17	–6.44	5.102–5.322
D	2.02	–6.02	5.163–5.405
E	1.55	–4.90	2.566–2.608
F	1.86	–6.57	1.516–1.538
G	1.63	–6.65	0.453–0.491
H	1.72	–7.20	0.375–0.407

Table 4 Best-fit results of experimental data according to *PSR* model

Samples	$\alpha \times 10^{-2}$ (N/μm)	$\beta \times 10^{-3}$ (N/μm^2)	H_{PSR} (GPa)	H_V (GPa)
A	1.92	0.66	1.223	1.997–2.068
B	–0.54	2.58	4.784	4.345–4.549
C	–0.77	3.12	5.785	5.102–5.322
D	–0.12	2.68	4.969	5.163–5.405
E	1.75	0.98	1.817	2.566–2.608
F	0.26	0.76	1.409	1.516–1.538
G	0.48	0.19	0.352	0.453–0.491
H	0.37	0.17	0.315	0.375–0.407

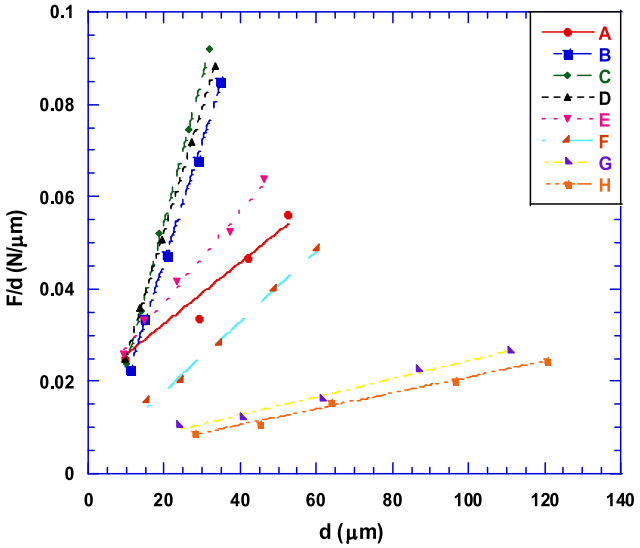

Fig. 5 Plots of F/d versus d for the samples

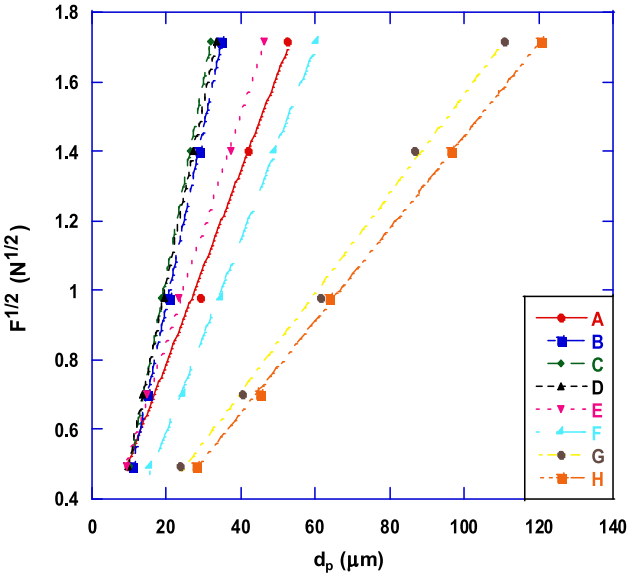

Fig. 6 Plots of diagonal length versus square root of applied loads for the samples

Table 5 The calculated load independent H_v, E, Y, and K_{IC} for the samples

Samples	E_0 (GPa)	Y_0 (GPa)	K_{IC} (Pa/m$^{1/2}$)	H_V (GPa)
A	100.24	0.407	1961.9	1.997–2.068
B	392.11	1.594	–2057.9	4.345–4.549
C	474.16	1.928	–2702.7	5.102–5.322
D	407.28	1.656	–988.67	5.163–5.405
E	148.92	0.605	583.08	2.566–2.608
F	115.49	0.469	774.95	1.516–1.538
G	28.85	0.117	526.27	0.453–0.491
H	25.81	0.105	437.03	0.375–0.407

is an important mechanical property of ceramic materials. It is a vital parameter in choosing materials for technological applications. For samples obeying *RISE* behavior, the microhardness values are higher when compared to other samples because there is no elastic recovery. Since elastic modulus, yield strength and fracture toughness depend on the values of microhardness, the increase in their values is expected. For samples obeying *ISE* behavior, elastic deformation as well as plastic deformation is observed. Namely, after the indenter is removed there is loosening in the sample surface. This causes a decrease in the microhardness of the sample. Toughness also decreases along with microhardness. The results of our samples are consistent with the results reported in the literature [17].

3.4.3 *Analysis According to Elastic/Plastic Deformation Model*

Bull et al. proposed that the dependence of indentation size on the applied load is given as [18, 19]

$$F = A_2(d_p + d_e)^2 \tag{10}$$

Table 6 Best-fit results of experimental data according to *EPD* model

Samples	A_2 (N/μm^2)	d_e (μm)	H_{EPD} (GPa)	H_V (GPa)
A	0.027	0.23	1.351	1.997–2.068
B	0.050	–0.06	4.636	4.345–4.549
C	0.056	–0.07	5.815	5.102–5.322
D	0.051	–0.01	4.823	5.163–5.405
E	0.032	0.20	1.898	2.566–2.608
F	0.027	0.04	1.351	1.516–1.538
G	0.014	0.13	0.363	0.453–0.491
H	0.013	0.11	0.313	0.375–0.407

Here A_2 is a constant and d_e is related to d_p plastic deformation. The values of A_2 and d_e are calculated from $F^{1/2} - d_p$ graph (Fig. 6).

The load independent microhardness value is calculated using;

$$H_{EPD} = 1854.4A_2 \tag{11}$$

As seen in Table 6, the calculated d_e values for samples B, C and D are negative. That means no elastic deformation is observed. Elastic deformation is observed only for samples A, E, F, G and H obeying *ISE* behavior. These samples obey

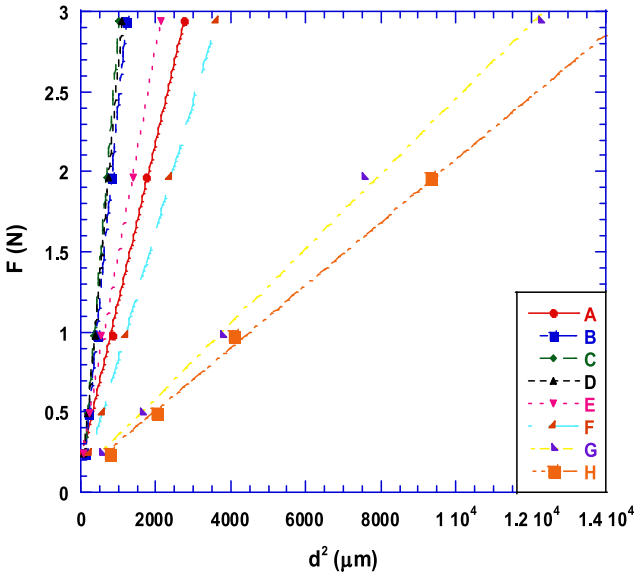

Fig. 7 Applied load vs. the square of the impression semi-diagonal length for the samples

ISE behavior because elastic deformation along with plastic deformation is observed in these samples.

3.4.4 Analysis Due to Hays–Kendall Approach

To analyze *ISE*, Hays–Kendall proposed that only elastic deformation develops in the samples for applied load values below a certain limit, but above the limit plastic deformation is observed [20]. Gane and Bowden observed that the indenter does not penetrate to some materials up to a certain value of applied load, and above the critical value of load it abruptly penetrates [21]. The indentation size does not increase although the applied load increases up to a critical applied load value. Hays-Kendall observed that the indentation size depends on an effective applied load $F_{\text{eff}} = F - W_{\text{HK}}$ instead of the applied load itself:

$$F - W_{\text{HK}} = A_{1\text{HK}} d^2 \tag{12}$$

where A_1 is a constant independent of the applied load. The values of W and A_1 are calculated from F–d^2 graph. The load independent hardness is calculated using

$$H_{\text{HK}} = 1854.4 A_{1\text{HK}} \tag{13}$$

The slope of the graph in Fig. 7 gives the value of $A_{1\text{HK}}$. In Table 7 the calculated values of load independent microhardness H_{HK}, W_{HK} and $A_{1\text{HK}}$ are tabulated.

The negative value of W_{HK} can be interpreted as the applied load being adequate to generate plastic deformation but it is inadequate to create elastic deformation [22]. In our study elastic deformation is observed only for samples A, E, F, G and H. No elastic deformation is observed for the other samples.

Table 7 Best-fit results of experimental data according to *HK* model

Samples	$A_{1\text{HK}} \times 10^{-5}$	W_{HK} (N)	H_{HK} (GPa)	H_V (Plateau Region) (GPa)
A	99.93	0.189	1.853	1.997–2.068
B	247.5	–0.060	4.590	4.345–4.549
C	293.3	–0.068	5.439	5.102–5.322
D	266.1	–0.012	4.936	5.163–5.405
E	128.9	0.190	2.390	2.566–2.608
F	80.25	0.030	1.488	1.516–1.538
G	23.34	0.120	0.432	0.453–0.491
H	19.55	0.118	0.362	0.375–0.407

For the samples obeying *ISE* behavior, microhardness values computed due to HK model are closer to those at the plateau region when compared to other models. As mentioned before, the load independent microhardness values are expected to be close to those at the plateau region [10, 23, 24]. Therefore, the Hays-Kendall model is the most suitable model for the analysis of the microhardness values and mechanical properties of the samples A, E, F, G and H. For the samples obeying *RISE* behavior, the models used above did not produce microhardness values close to the ones of the plateau region. Indentation-Induced Cracking (*IIC*) Model is another model to be used for the analysis of mechanical properties of the samples obeying *RISE* behavior.

3.4.5 Analysis Due to Indentation-Induced Cracking (IIC) Model

It is a model proposed by Li and Bradt for the analysis of the microhardness of materials obeying *RISE* behavior [25]. According to this model, the applied load is balanced by the total sample resistance at the maximum depth. The sample resistance is composed of four components

1. The slipping of the sample or the indenter at the interfaces.
2. Elastic deformation.
3. Plastic deformation.
4. Cracks in the sample.

According to Li and Bradt friction (slipping) and elastic effects produce *ISE* behavior, and the indentation cracking produces *RISE* behavior. The microhardness value is calculated using the following equation:

$$H_v = \lambda_1 K_1 \left(\frac{F}{d^2}\right) + K_2 \left(\frac{F^{5/3}}{d^3}\right) \tag{14}$$

where d is the indentation size, and λ_1, K_1, K_2 are constants. K_2 depends on the applied load, while K_1 depends on the geometry of the indenter.

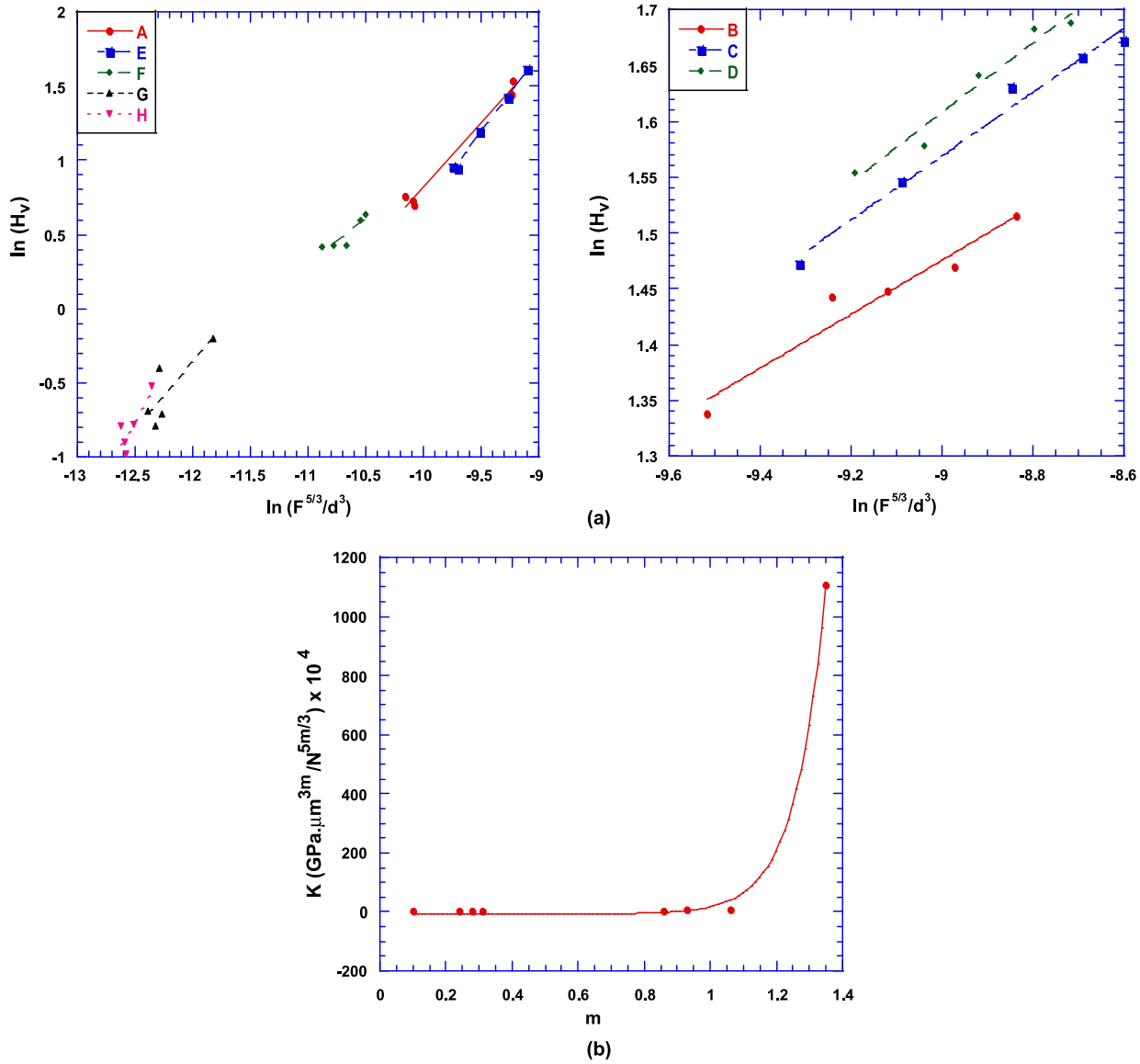

Fig. 8 (**a**) Variation of $\ln H_V$ with $\ln(F^{5/3}/d^3)$ according to *IIC* model for all samples, (**b**) the correlation between the *IIC* model parameters K and m for all samples

Table 8 Best-fit results of experimental data according to *IIC* model

Numune	m	$K \times 10^4$ $(N^{(3-5m)/3}/\mu m^{(2-3m)})$	H_{IIC} (GPa)	H_V (GPa)
A	0.86	1.3200	3.209	1.997–2.068
B	0.24	0.0038	4.246	4.345–4.549
C	0.28	0.0062	5.131	5.102–5.322
D	0.31	0.0083	5.210	5.163–5.405
E	1.06	8.0010	3.419	2.566–2.608
F	0.62	0.0914	1.729	1.516–1.538
G	0.93	4.9020	1.471	0.453–0.491
H	1.35	1107.2	0.502	0.375–0.407

Table 9 The results of load dependent Vickers microhardness at the plateau region and load independent hardness values calculated using *PSR*, *MPSR*, *EPD* and *HK* models

Samples	H_V (GPa) (in plateau region)	H_{PSR} (GPa)	H_{EPD} (GPa)	H_{HK} (GPa)	H_{IIC} (GPa)
A	1.997–2.068	1.223	1.351	1.853	3.209
B	4.345–4.549	4.784	4.636	4.590	4.246
C	5.102–5.322	5.785	5.815	5.439	5.131
D	5.163–5.405	4.969	4.823	4.936	5.210
E	2.566–2.608	1.817	1.898	2.390	3.419
F	1.516–1.538	1.409	1.351	1.488	1.729
G	0.453–0.491	0.352	0.363	0.432	1.471
H	0.375–0.407	0.315	0.313	0.362	0.502

For an ideal plastic material $H_v = K_1(F/d^2)$, $\lambda_1 = 1$ and $K_2(F^{5/3}/d^3) = 0$. For perfect brittle solids $H_v = K_2(F^{5/3}/d^3)$ and $\lambda_1 = 0$. In the (14) we can take $d = 7h$. This equality is associated with the angle (148 °) between the opposite sides of the indenter, and h is the depth of the indentation. For brittle materials the second part of the equation is used. In our PbSe added samples no elastic deformation is observed, which means they are brittle. Therefore, (15) derived from (14) is to be used to calculate the hardness values of our samples. We have

$$H_v = K\left(\frac{F^{5/3}}{d^3}\right) \tag{15}$$

where K and m are load independent constants whose values are calculated from $\ln(H_v) - \ln(F^{5/3}/d^3)$ graph (Fig. 8a). The value of m is a measure of *ISE*. For $m > 0.6$ the sample obeys *ISE* behavior, while for $m < 0.6$ the sample obeys *RISE* behavior [17, 22].

Since no elastic deformation is observed in the hardness analysis of samples B, C and D this model produced the best results for samples obeying *RISE* behavior. The values of m calculated using the slope of the graph are tabulated in Table 8. In the table $m < 0.6$ for samples B, C and D while $m > 0.6$ for samples A, E, F, H, G. We see that the samples B, C and D obey *RISE*, while samples A, E, F, G and H obey *ISE* behavior. The value of m increases for both PbSe added Bi-2212 crystallines and glass samples with addition ratio.

The fitting of the graph in Fig. 8b gives an empirical relation between K and m like

$$K = 21.22e^{11.06m}$$

4 Conclusion

The effect of PbSe addition on the mechanical properties of Bi-2212 superconductor is analyzed. XRD measurements are taken to determine the crystal structure and lattice parameters, SEM micrographs are used to determine surface morphology and grain sizes. Vickers microhardness measurements are made to determine the mechanical properties of the samples. For glass samples the microhardness increases with increasing PbSe addition, while for superconducting samples microhardness decreases with PbSe addition. The experimental results of the microhardness measurements are analyzed using Kick's law, PSR, EPD, Hays–Kendall and IIC models. After employing the above mentioned models, we conclude that the Hays–Kendall model is suitable for samples obeying *ISE* behavior (A, E, F, G, H) and IIC model is suitable for samples obeying *RISE* behavior (B, C, D). These results are summarized in Table 9. XRD results show that the Bi-2212 phase ratio, c lattice parameter and grain size increase in superconducting samples, while the lattice parameter a decrease with addition. The increase in average grain sizes is also verified by SEM analysis. The increase in the grain sizes results in the decrease in porosity among grains and better crystallinity of the samples.

Acknowledgements The Authors thank the financial support for this work through the Scientific Research Projects (BAP 05/2011-48) Foundation of Gazi University Ankara.

References

1. Uzun, O., Kölemen, U., Çelebi, S., Güçlü, N.: Journal of European Ceramic Society **25**(6), 969–977 (2005)
2. Asikuzun, E., Ozturk, O., Cetinkara, H.A., Yildirim, G., Varilci, A., Yılmazlar, M., Terzioglu, C.: J. Mater. Sci., Mater. Electron. (2011). doi:10.1007/s10854-011-0537-0
3. Uzun, O., Karaaslan, T., Keskin, M.: Journal of Alloys and Compounds **358**, 104–111 (2003)
4. Yoshino, Y., Iwabuchi, A., Onodera, R., Chiba, A., Katagiri, K., Shimizu, T.: Cryogenics **41**, 505–511 (2001)
5. Gong, J., Wu, J., Guan, Z.: Journal of the European Ceramic Society. **19**, 2625–2631 (1999)
6. Elmustafa, A.A., Stone, D.S.: J. Mech. Phys. Solid **51**, 357 (2003)
7. Khalil, S.M.: Journal of Physics and Chemistry of Solids **64**, 855 (2003)
8. Sangwal, K., Borc, J., Kavetskyy, T.: Journal of Non-Crystalline Solids **357**, 3117–3122 (2011)
9. Gong, J.H., Wu, J.J., Guan, Z.: Mater. Lett. **38**, 197 (1999)
10. Quınn, J.B., Quınn, V.D.: Journal of Materials Science **32**, 4331–4346 (1997)
11. Ozturk, O., Erdem, M., Asikuzun, E., Yildiz, O., Yildirim, G., Varilci, A., Terzioglu, C.: J. Mater. Sci., Mater. Electron. (2012). doi:10.1007/s10854-012-0722-9

12. Ozturk, O.: J. Matter Sci., Mater. Electron. (2011). doi:10.1007/s10854-011-0580-x
13. Li, H., Bradt, R.C.: Journal of Materials Science **28**, 917–926 (1993)
14. Leenders, A., Mich, M., Freyhard, H.C.: Physica C **279**, 173 (1997)
15. Yilmazlar, M., Ozturk, O., Gorur, O., Belenli, I., Terzioglu, C.: Supercond. Sci. Technol. **20**, 365–371 (2007)
16. Ozturk, O., Cetinkara, H.A., Asikuzun, E., Akdogan, M., Yilmazlar, M., Terzioglu, C.: J. Mater Sci: Mater Electron **22**, 1501–1508 (2011)
17. Sangwal, K.: Materials Chemistry and Physics **63**, 145–152 (2000)
18. Upit, G.P., Varchenya, S.A.: Phys. Status Solidi A **17**, 831 (1966)
19. Bull, S.J., Page, T.F., Yoffe, P.E.H.: Mag. Lett. **59**, 281 (1989)
20. Hays, C., Kendall, E.G.: Metallurgy **6**, 275–282 (1973)
21. Gane, N., Bowden, F.P.: Journal of Applied Physics **39**, 1432–1435 (1968)
22. Awad, R., Abou-Aly, A.I., Kamal, M., Anas, M.: J. Supercond. Nov. Magn. **24**, 1947–1956 (2011)
23. Gong, J., Zhao, Z., Guan, Z., Mıao, H.: Journal of the European Ceramic Society **20**, 1895–1900 (2000)
24. Peng, Z., Gong, J., Mıao, H.: Journal of European Ceramic. Society **24**, 2193–2201 (2004)
25. Li, H., Bradt, R.C.: J. Mater. Sci. **31**, 1065 (1996)